

Generation and Progress Behavior of Strain-Induced Abnormally Large Grains in Superalloy 718



CHUYA AOKI, MASAYOSHI DATE, TOMONORI UENO, TAKEHIRO OHNO,
and KATSUNARI OIKAWA

Herein, the behavior associated with strain-induced abnormally large grains in superalloy 718 was investigated using compression testing and subsequent heat treatment below the δ -phase solvus temperature of 980 °C. The nuclei of abnormally large grains included some grains that were newly recrystallized through nucleation. Abnormally large grains were caused by a difference in intragranular misorientation between the dynamic recrystallized grains and the deformed matrix. The initiation of abnormally large grains was retarded in response to a decrease in plastic strain, leading to the formation of microstructures consisting of larger grains with a more complex morphology. Grain boundaries migrated locally in a direction perpendicular to, or predominantly in a direction parallel to, the $\Sigma 3$ {111} twin boundaries, along with the high-order twin formation. To determine the direction parallel to the $\Sigma 3$ {111} twin boundaries, the regions where parent grain and dissimilar twin growth occurred in the same direction along their twin boundaries were analyzed using {110} PFs. The growth direction consisted of only one set of common $\langle 110 \rangle$ axes such that the arrangement of atoms was consistent. Owing to multiple twinning, abnormally large grains seemed to evolve in varying growth directions.

<https://doi.org/10.1007/s11661-020-05838-6>

© The Minerals, Metals & Materials Society and ASM International 2020

I. INTRODUCTION

SUPERALLOY 718 is a nickel-based alloy widely used for applications such as in the manufacture of parts for aircraft engines and power generation turbines. These technologies typically require alloys with a fine-grained microstructure to achieve high fatigue lifetimes. The manufacture of superalloy 718 involves the use of hot-working processes at temperatures below the δ -phase solvus temperature (950 °C to 1010 °C) to control the microstructure. Particles that form during the δ phase inhibit the grain growth of the matrix after recrystallization, thus ensuring a fine-grained microstructure and good fatigue-resistant properties.^[1] However, abnormally large grains often occur, which causes the matrix grains to become coarse. It was previously reported that prior exposure to low plastic

strains caused coarse-grained structure during heat treatment below the δ -phase solvus temperature,^[2–8] thereby decreasing the low-cycle fatigue lifetime.^[9] Abnormally large-grained microstructure has also been observed in other superalloys.^[10–13] Such strain-induced grain coarsening has often been reported as abnormal grain growth (AGG). However, this phenomenon has been considered a primary recrystallization process caused by stored strain energy.^[5,11,13] Such formation of abnormally large grains has also been observed in electrical steel^[14,15] and materials created through grain boundary engineering^[16–18] to improve intergranular corrosion, termed twin-related domains (TRDs) due to the formation of a heavily twinned microstructure.^[19–21]

Generally, annealing twins tend to be formed in the recrystallization of face-centered-cubic (fcc) metals and alloys with low stacking-fault energy. There are various theories to explain the twinning mechanism of fcc crystals, with representative models including the growth accident model,^[22,23] grain encounter model,^[24] and grain boundary dissociation model.^[25] In the growth accident model, grain boundary migration causes atoms to move across grain boundaries and a build-up fault occurs by which atoms stack in a close-packed plane, thereby forming a twin crystal. This is the most well-supported theory at present. Gleiter^[22] suggested that atoms are stacked on {111} planes, in particular {111} facet planes, resulting in the formation of annealing twins that cause an atom build-up

CHUYA AOKI is with Yasugi Works, Engineering & Solutions Department, Hitachi Metals, LTD., 2107-2 Yasugi-cho, Yasugi, Shimane 692-8601, Japan. Contact email: chuuya.aoki.vb@hitachi-metals.com MASAYOSHI DATE, TOMONORI UENO, and TAKEHIRO OHNO are with Metallurgical Research Laboratory, Hitachi Metals, LTD., 1240-2 Hashima, Yasugi, Shimane 692-8601, Japan. KATSUNARI OIKAWA is with the Department of Metallurgy Graduate School of Engineering, Tohoku University, Aoba-6-6-02, Aramaki, Aoba-ku, Sendai, Miyagi 980-8579, Japan.

Manuscript submitted April 24, 2019.
Article published online May 30, 2020

fault on the closely packed planes. Mahajan *et al.*^[23] also advocated the growth accident model but considered the atomic stack to occur not on {111} facet planes but on {111} step planes intersecting with {111} facet planes. They suggested that a Shockley partial dislocation loop, including a stacking fault, was swept from the step surface into the grain and that annealing twins were formed due to the continuous overlap of stacking faults. The grain encounter model of Burgers *et al.*^[24] proposes that when a growing grain encounters a matrix region that happens to possess a twin orientation, the stimulation causes a twin crystal to be generated. In the grain boundary dissociation model of Meyers and Murr,^[25] it is proposed that annealing twins that are generated from the ledge of a grain boundary will develop into the grain and that the high-angle grain boundary will degrade into a low-energy twin boundary or low-angle grain boundary. This lowers the energy of the system and annealing twins are formed without the associated grain boundary movement.

Barr *et al.*^[20] investigated the twinning mechanism in the TRD coarsening process of austenitic stainless steel 316L and clarified that twin boundaries formed behind the migrating grain boundary front, which is parallel to the {111} planes. They reported this based on the growth accident model of Gleiter.^[22] Jin *et al.*^[26] worked the influence of the stored strain energy level on annealing twin formation of pure Ni and proposed that the tortuosity of the recrystallization front tended to increase the probability of segments parallel to {111} planes. We demonstrated that the abnormally large-grained structure of superalloy 718 was accompanied by an increase in the twin boundary ratio (calculated as a length of twin boundaries divided by the overall boundary length), but the correlation of the abnormally large grains with the formation of twin boundaries was still unclear.^[7,8] This present study has been undertaken with the aim of investigating the detailed mechanisms of the generation and progress of abnormally large grains through careful observation of the microstructures.

II. EXPERIMENTAL PROCEDURES

The superalloy 718 billet (Fe-54Ni-18Cr-3-Mo-0.5Al-1Ti-5.4Nb-0.025C, mass pct) was forged into disks through upset forging and subsequent ring rolling at 980 °C (below the δ -phase solvus temperature). Coupons were cut from the ring-rolled material, such that the compression axis was parallel to the tangential direction. In this study, we used two types of double-cone specimens^[10] that differed in size, as shown in Figure 1. Process diagrams detailing the particulars of the test conditions are shown in Figure 2. Specimen A (Figure 1(a)) was machined from coupons that had been pre-heat-treated at 980 °C for 1 hour before being subjected to the compression test in a servohydraulic facility equipped with an induction heating system. The initial microstructure of the sample pre-heat-treated at 980 °C was a fine-grained structure with grain size of $\sim 12 \mu\text{m}$. The δ -phase particles, comprising ~ 5 pct of the area, were homogeneously distributed, as demonstrated in our previous study.^[7,8] After the specimen A

samples were heated at 980 °C, they were deformed at 980 °C, with a 10 to 30 pct reduction in height at a constant displacement rate of 7 mm/s (nominal strain rate of 0.5 s^{-1}), and subsequently annealed at 980 °C for 0 to 240 seconds. Specimen B (Figure 1(b)) was machined from coupons that had not been exposed to preheat treatment (because of later heating for hot compression) and then subjected to the compression test using a hydraulic facility equipped with resistance-heated forging dies. Specimen B samples were deformed upon heating at 980 °C for 1 hour, exhibiting a 12 pct reduction in height at a constant displacement rate of 42 mm/s (nominal strain rate 0.5 s^{-1}) or 0.42 mm/s (nominal strain rate 0.005 s^{-1}), with upper and lower dies heated to approximately 980 °C, followed by water quenching. Solution heat treatment was subsequently carried out at 980 °C for 1 hour.

Figure 3 shows a flow diagram describing the process of microstructure evaluation. The specimens were cut in half along the longitudinal axis after deformation and subsequent annealing and solution heat treatment, and were then polished to allow observation of the microstructures of the longitudinal sections. As shown in Figure 3(a), the microstructures of the deformed and annealed specimen A samples were observed using electron backscatter diffraction (EBSD; Digiview 4, EDAX). The EBSD scans were performed with a step size of $0.2 \mu\text{m}$ using a scanning electron microscope (SEM; ULTRA 55, Carl Zeiss AG Corporation) equipped with an EBSD detector. The grain size, intragranular misorientation, grain shape circularity, and crystallographic orientation were evaluated by analyzing EBSD datasets using the TSL OIM analysis software 7 program (TSL Solutions). The average grain size was calculated by the area-weighted grain distribution. Intragranular misorientation was evaluated using grain orientation spread (GOS), which is defined as the average intragranular misorientation of each measurement point with respect to all measurement points in the grain

$$\text{GOS} = \frac{1}{n} \sum_i^n (\theta_i - \theta_{\text{AVE}}), \quad [1]$$

where θ_i , θ_{AVE} , and n are the orientation of measurement point i in a grain, the average orientation of the grain, and the total number of measurement points in the grain, respectively. The minimum boundary misorientation angle of the low-angle boundaries was set to 2 deg, which is the critical angle for recognizing boundaries among pairs of measurement points. Twin boundaries are defined by a misorientation of 60 deg along the axis $\langle 111 \rangle$ with a tolerance of 8.66 deg (Brandon's criterion^[27]). Grain shape circularity, C_g , is a dimensionless value representing the degree to which the grain is similar to a circle, taking into consideration the smoothness of the perimeter, and is defined as

$$C_g = \frac{4\pi A_g}{p_g^2}, \quad [2]$$

where A_g is the area of the grain and p_g is the perimeter of the grain. Grains that intersected with the edge of the

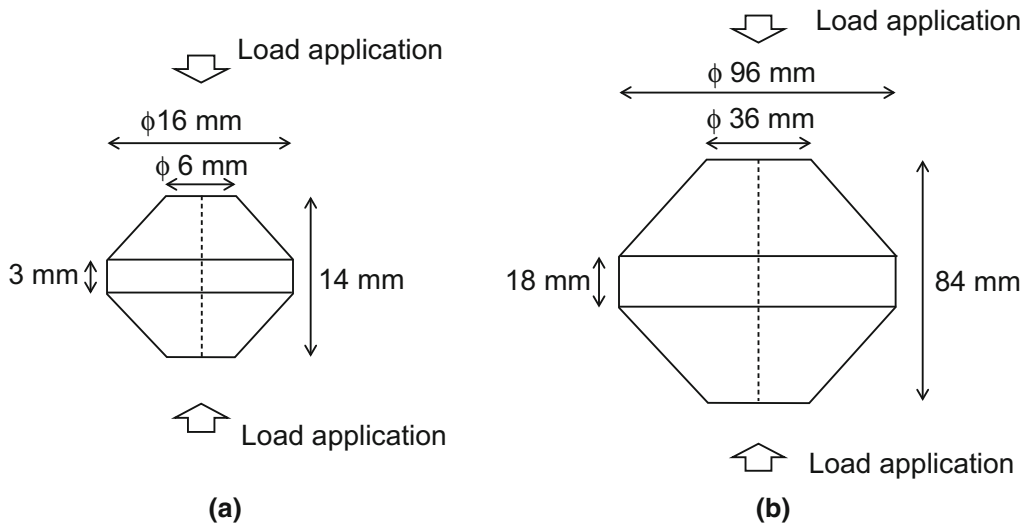


Fig. 1—Illustration of the geometry of the double-cone specimens: (a) specimen A and (b) specimen B.

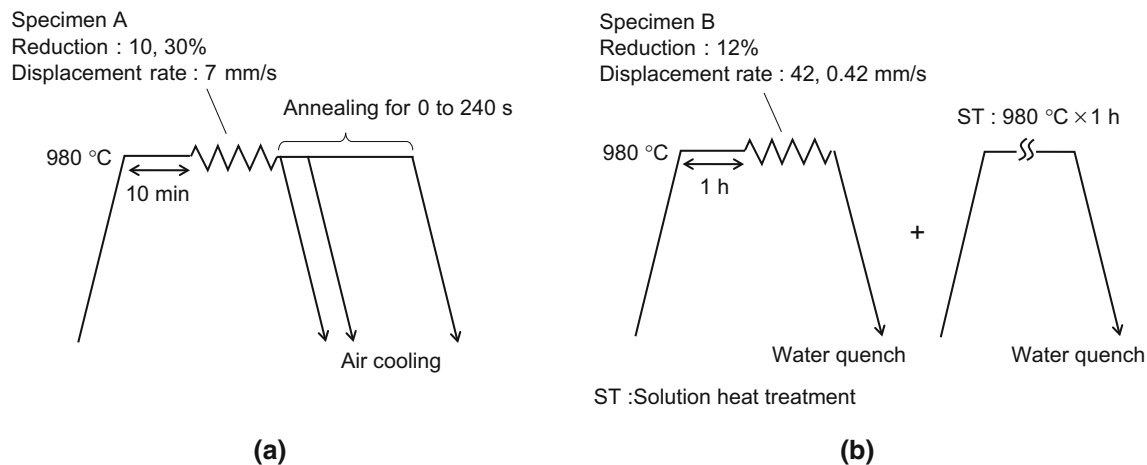


Fig. 2—Process diagrams detailing the test conditions: (a) compression test and annealing immediately after deformation (specimen A) and (b) compression test and solution heat treatment (specimen B).

measurement area were not included for the purposes of this analysis.

As shown in Figure 3(b), the microstructure of the deformed specimen B samples was observed using a transmission electron microscope (TEM; JEM-2100-PLUS, JEOL*) and EBSD (Hikari SUPER, EDAX)

*JEOL is a trademark of Japan Electron Optics Ltd., Tokyo.

with *in-situ* annealing. The TEM examination was conducted at an accelerating voltage of 200 kV. The extracted samples for EBSD measurement (with a step size of 0.6 μm) with *in-situ* annealing were mechanically polished using colloidal silica to achieve a mirror surface and then annealed in an SEM (JSM-7001F, JEOL) chamber at 980 °C. The microstructure of specimen B samples after solution heat treatment was also observed using an optical microscope and EBSD (Digiview 4, EDAX).

III. RESULTS

A. Behavior of Microstructural Evolution

Detailed microstructural observation of the deformed specimen A during annealing was carried out to ascertain the behavior of the microstructural evolution. Figure 4 shows GOS maps overlaid with maps of both the grain boundaries and the $\Sigma 3$ twin boundaries with respect to different plastic strains and annealing times. It was observed that the microstructural evolution during annealing was accompanied by a decrease in GOS, which was related to stored strain energy within the grains. In addition, the decrease in GOS slowed with decreasing plastic strain because a high-GOS region remained in the low-strain sample after 60 seconds (Figure 4(a)). Recrystallized grains with low GOS were observed at plastic strains of 0.26 and 0.58 in the as-deformed sample (annealing time 0 seconds), as shown in Figures 4(c) and (d). The GOS distribution of the microstructure shown in Figure 4(c) that was

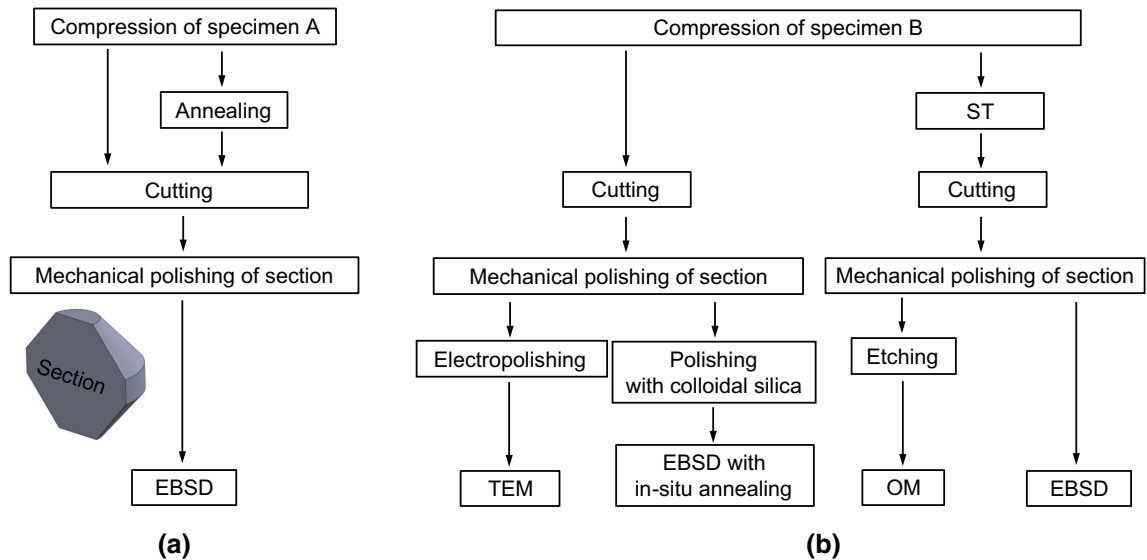


Fig. 3—Flow diagram describing the microstructural evaluation of the samples: (a) specimen A and (b) specimen B.

annealed for 0 seconds (partial recrystallization) and 60 seconds (almost complete recrystallization) is shown in Figure 5. The median value of GOS decreased in the range of approximately 3 to 0.4 deg with the progress of the recrystallization process. Recrystallized grains were defined as grains having a GOS below 0.8 deg for the purposes of this study. It was noted that small grains with low GOS appeared, even at low plastic strains of 0.1 and 0.07, as indicated by the black arrows in Figures 4(a) and (b). Such low plastic strains might form the nuclei of the abnormally large-grained microstructure, as mentioned in our previous study.^[8] Figure 6 shows the TEM micrographs of the microstructure at a position corresponding to a plastic strain of 0.1 for the specimen B sample deformed at 980 °C at a displacement rate of 42 mm/s, indicating that the low dislocation-free grains shown in Figures 6(a) through (c) were created in the deformed matrix with high-density dislocation, as shown in Figure 6(d). These results suggest that the strain-induced abnormal grain coarsening is a primary recrystallization phenomenon that is caused by stored strain energy, as mentioned by Agnoli *et al.*^[5] for Inconel 718, Miller *et al.*^[11] for René 88DT, and Charpagne *et al.*^[13] for René 65. Moreover, Figure 6 demonstrates that the nuclei of abnormally large grains appear to be the nucleation of newly recrystallized grains.

As shown in Figures 4(a) through (d), the decrease in GOS, namely, the progress of recrystallization at a low plastic strain of 0.07 (Figure 4(a)) during annealing, is slower than that at higher plastic strains (Figures 4(b) through (d)). However, a low plastic strain of 0.07 exceeds the lower limit ($\varepsilon = 0.05$) for the occurrence of abnormally large grains when deformed at a nominal strain rate of 0.5 s^{-1} .^[7,8] Recrystallization proceeds relatively well during annealing for 60 seconds (Figure 4(a)). This microstructure evolution is likely to be faster compared to the data available in the literature, which indicated that there are clearly two populations of

fine and overgrown grains at the position corresponding to a low plastic strain of 0.07 during annealing for 2 hours.^[5] Such microstructure having two populations of fine and overgrown grains forms at the position corresponding to the lower limit of the plastic strain range for the occurrence of abnormally large grain. As stated in our previous study,^[8] the deformation at a low strain rate shifts the critical plastic strain at which abnormally large grains occur to higher plastic strains, compared to the deformation at a high strain rate.

Figure 7(a) indicates the change in size of recrystallized grains formed after deformation during annealing. Compared to the cases involving plastic strains of 0.26 and 0.58, the small grains recrystallized after exposure to plastic strains of 0.07 and 0.1 became larger with annealing time. In addition, Figure 7(b) indicates the change in shape circularity, C_g , of recrystallized grains during annealing. Compared to the cases involving plastic strains of 0.26 and 0.58, the small grains recrystallized after exposure to plastic strains of 0.07 and 0.1 became more irregular in shape (low C_g) with annealing time. Figures 7(a) and (b) implied that the formation of abnormally large grain is accompanied by a complex boundary migration.

B. Behavior of Twin Boundary in Abnormally Large Grain

The correlation between crystal orientation and morphology of the recrystallized grains of specimen B was investigated. Figures 8(a) and (b) are the macrographs showing the evaluated positions of the solution-heat-treated specimen B after 12 pct reduction deformation at 980 °C and at displacement rates of 42 and 0.42 mm/s, respectively. It is observed that the deformation at low displacement rate shifts the critical plastic strain at which abnormally large grains occur to higher strains, compared to the deformation at high displacement rate. From this, it can be interpreted that

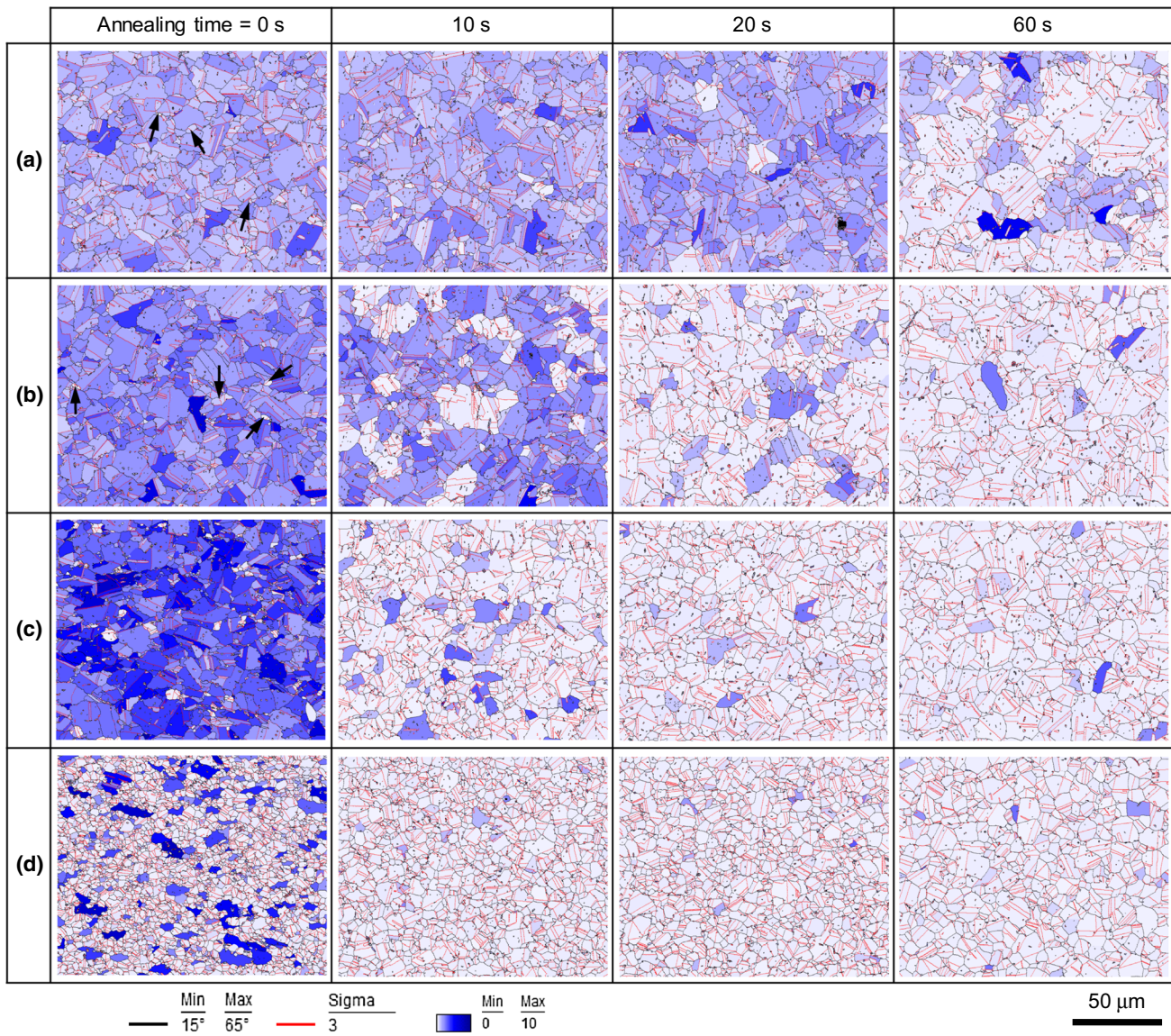


Fig. 4—GOS maps overlaid with grain boundaries and twin boundaries for the microstructure of specimen A deformed at 980 °C at a displacement rate of 7 mm/s and subsequently annealed at 980 °C for 0, 10, 20, and 60 s: (a) $\epsilon = 0.07$, (b) $\epsilon = 0.1$, (c) $\epsilon = 0.26$, and (d) $\epsilon = 0.58$.

the strain rate greatly influences the stored strain energy distribution, leading to the difference in the plastic strain range inducing abnormally large grains, as mentioned in our previous study.^[7,8]

Figure 9 shows the inverse pole figure (IPF) colored orientation map for the abnormally large grains containing twins in the solution-heat-treated specimen B exposed to a plastic strain of 0.05 (Figure 8(a)). The different parent grains G1 and G2 were observed to contain several twins (T1 through T3 in G1, T4 and T5 in G2) in addition to evidence of local boundary migration. Figure 9 also shows the $\{111\}$ pole figures (PFs) for each parent grain and twin. A comparison

of the IPF map with the $\{111\}$ PFs of the grain G1 and the twins T1 through T3 seems to indicate that the local growth directions a, b, and c are consistent with each common $\langle 111 \rangle$ rotational axis of the grain G1 with the twins T1, T2, and T3, respectively. Similarly, the local growth direction of the grain G2 seems to correspond to the common $\langle 111 \rangle$ rotational axis (directions d and e) for the twins T4 and T5, respectively.

Figure 10 shows the IPF map for the abnormally large grain containing higher-order twins for the solution-heat-treated specimen B exposed to a plastic strain of 0.12 (Figure 8(b)). The parent grain G3 contained primary (T6), secondary (T7 and T8), and tertiary (T9)

twins in the abnormally large grain. Figure 10 also shows the $\{111\}$ and $\{110\}$ PFs for this parent grain and for each twin. Based on the IPF map and the $\{111\}$ PFs, the formation of the twins T8 and T9 produced a change

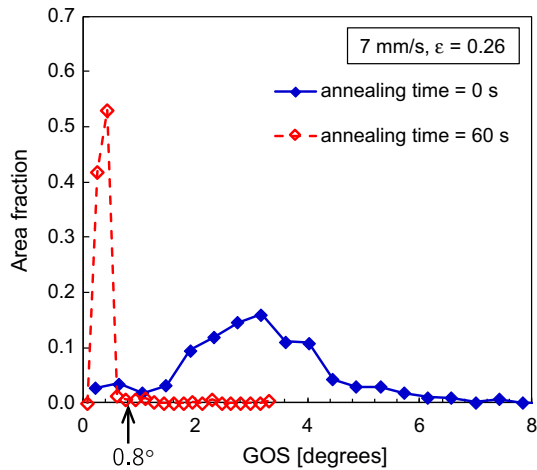


Fig. 5—GOS distribution of the microstructure at the location subjected to a plastic strain of 0.26 for deformed specimen A.

in the growth direction, which was perpendicular to the $\Sigma 3 \{111\}$ twin boundaries ($g \Rightarrow h$). In addition, the twin T6 that originated from the twin T7 partially surrounded the neighboring grain by growing in the direction f, as seen in the circled area on the IPF map shown in Figure 10. From observation of the abnormally large grains seen in Figures 9 and 10, it appeared that the abnormally large grains developed into a complex morphology accompanied by the formation of twins and growth in a direction perpendicular to the $\Sigma 3 \{111\}$ twin boundaries, which was similar to the results presented by Barr *et al.*^[18] However, it was observed that grain boundaries migrated predominantly in a direction parallel to the $\Sigma 3 \{111\}$ twin boundaries, as mentioned by Jin *et al.*^[26]

In order to identify the direction parallel to the $\Sigma 3 \{111\}$ twin boundaries, we focused on the rectangular area on the IPF map of Figure 10, which consisted of the parent grain G3, the primary twin T6, and the secondary twin T7. They possessed only one common $\langle 110 \rangle$ axis (direction j), as shown in the $\{110\}$ PFs of Figure 10. The growth in the direction parallel to the $\Sigma 3 \{111\}$ twin boundaries was also confirmed by *in-situ* annealing. Figure 11 shows the EBSD results measured during the *in-situ* annealing of the cut-out specimen B

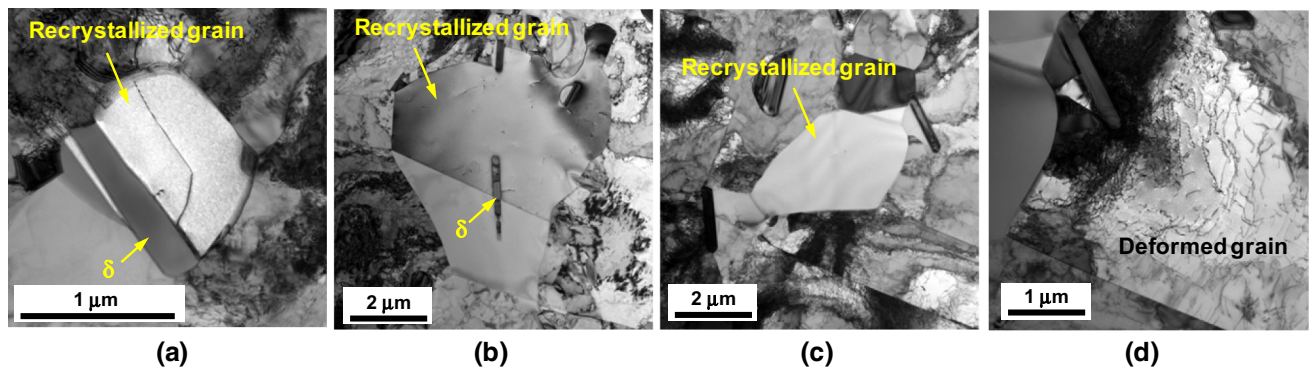


Fig. 6—TEM micrographs of the microstructure oriented to $[011]$ at the location subjected to a plastic strain of 0.1 for specimen B deformed at 980°C at a displacement rate of 42 mm/s : (a) through (c) recrystallized grain and (d) deformed grain (from Ref. [8] with permission).

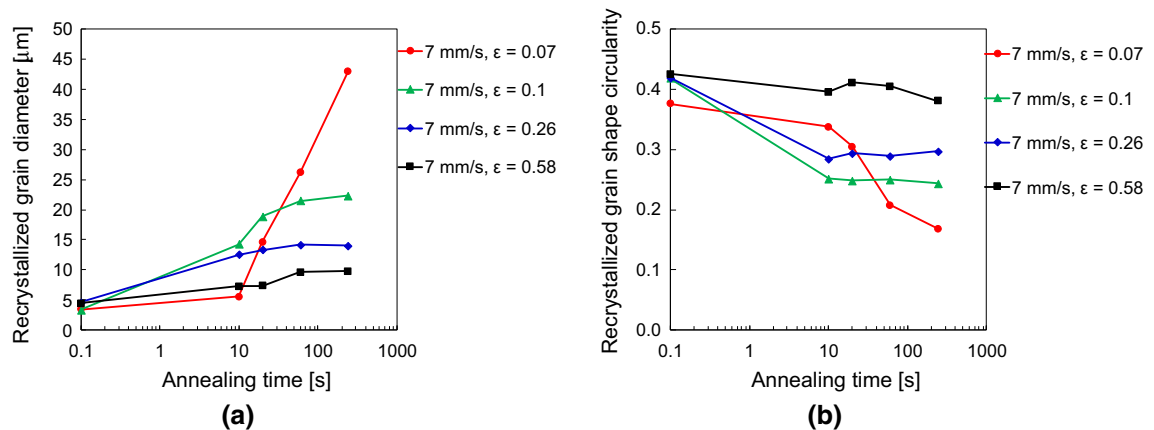
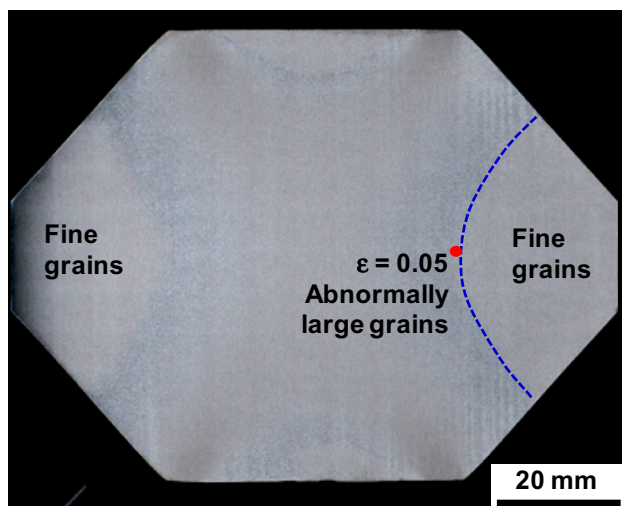
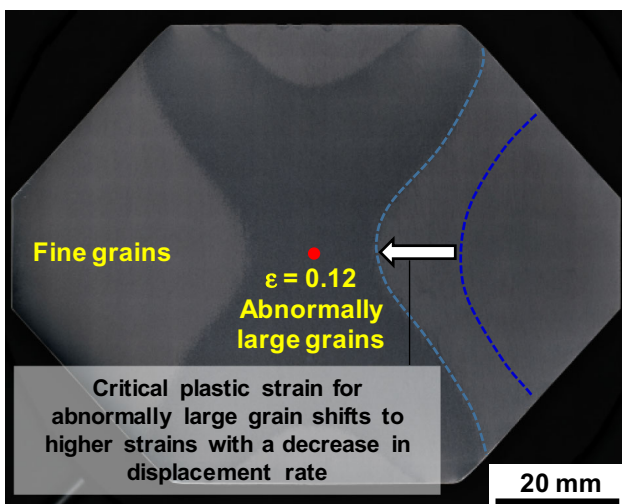


Fig. 7—Change in recrystallized grains during the annealing process for specimen A deformed at 980°C : (a) grain size and (b) grain shape circularity.



(a)



(b)

Fig. 8—Cross-sectional macrographs showing the EBSD measurement area for the solution-heat-treated specimen B after 12 pct reduction deformation at 980 °C. Displacement rate: (a) 42 mm/s and (b) 0.42 mm/s.

sample, that was exposed to a plastic strain of 0.12 and deformed at 980 °C at a displacement rate of 0.42 mm/s, in the SEM sample chamber. The parent grain G4 and the primary twins T10 and T11 appear to grow at 980 °C in a common $\langle 110 \rangle$ direction (direction n) for 35 minutes. The grain coarsening with the free surface of the sample is likely to be slower compared to that of the sample inside (Figures 4 and 11). In this study, based on three-dimensional information, which can be assessed from the measurement results of two-dimensional sections, we considered the migration direction of a grain boundary, as stated in Figures 9 through 11. However, it is necessary to investigate further observations in order to verify our assumption.

The coarsening of recrystallized grains may not only be due to grain boundary migration but may also be due to the replacement of the high-angle grain boundaries with low-angle grain boundaries through the formation of twins. Figure 12 shows the grain boundary image of the abnormally large grains shown in Figure 9 along with the misorientation and coincidence relationship between each analyzed point. It was observed that a high-angle boundary (blue line) between the parent grains G1 and G2 was partially converted to a low-angle boundary (green line), as indicated in areas 1 through 3. The misorientation between the parent grains G1 and G2 was a high angle of approximately 50 deg without a coincidence relationship. However, the twin T3 in the parent grain G1 possessed a low-angle boundary of approximately 12 deg to the neighboring grain G2 in areas 1 and 2. Similarly, the twin T12 in the parent grain G2 possessed a low-angle boundary to the neighboring grain G1 in area 3. This suggests that a coarse grain, including low-angle grain boundaries, would be formed as a result of the high-angle grain boundary changing to a low-angle grain boundary due to twin formation.

IV. DISCUSSION

It was found that the nuclei of strain-induced abnormally large grains were some grains that were newly recrystallized through nucleation after application of low plastic strain (Figure 6). In addition, it was observed that as the plastic strain decreased, the initiation of abnormally large grains was retarded and the final microstructure became coarser and displayed a more irregular morphology (Figures 4 and 7). Similar tendencies could be seen with respect to “normal” recrystallization, although there was a difference in extent. Abnormally large grains occurred beyond the δ -phase particles that were homogeneously dispersed, as demonstrated in our previous study.^[7,8] Hence, the driving force for grain boundary migration taking into account the stored strain energy appears to overcome the pinning force of δ -phase particles, as mentioned by Agnoli *et al.*^[4,5] From these results, it was apparent that the final microstructure was notably affected by both the fraction of recrystallization and the amount of stored strain energy in the deformed matrix. In the case of the strain-induced abnormally large grains, only a few recrystallized grains grew and formed a coarsened grain structure because of the lower frequency of impingement upon each other. In addition, the residual strain in the deformed matrix was lower compared with that of the normal partial recrystallization. While detecting the prior direction, it was noted that the partial boundary migration of the recrystallized grain resulted from the decreasing total energy in the system. The grains tended to become coarse and have a complex morphology as a result.

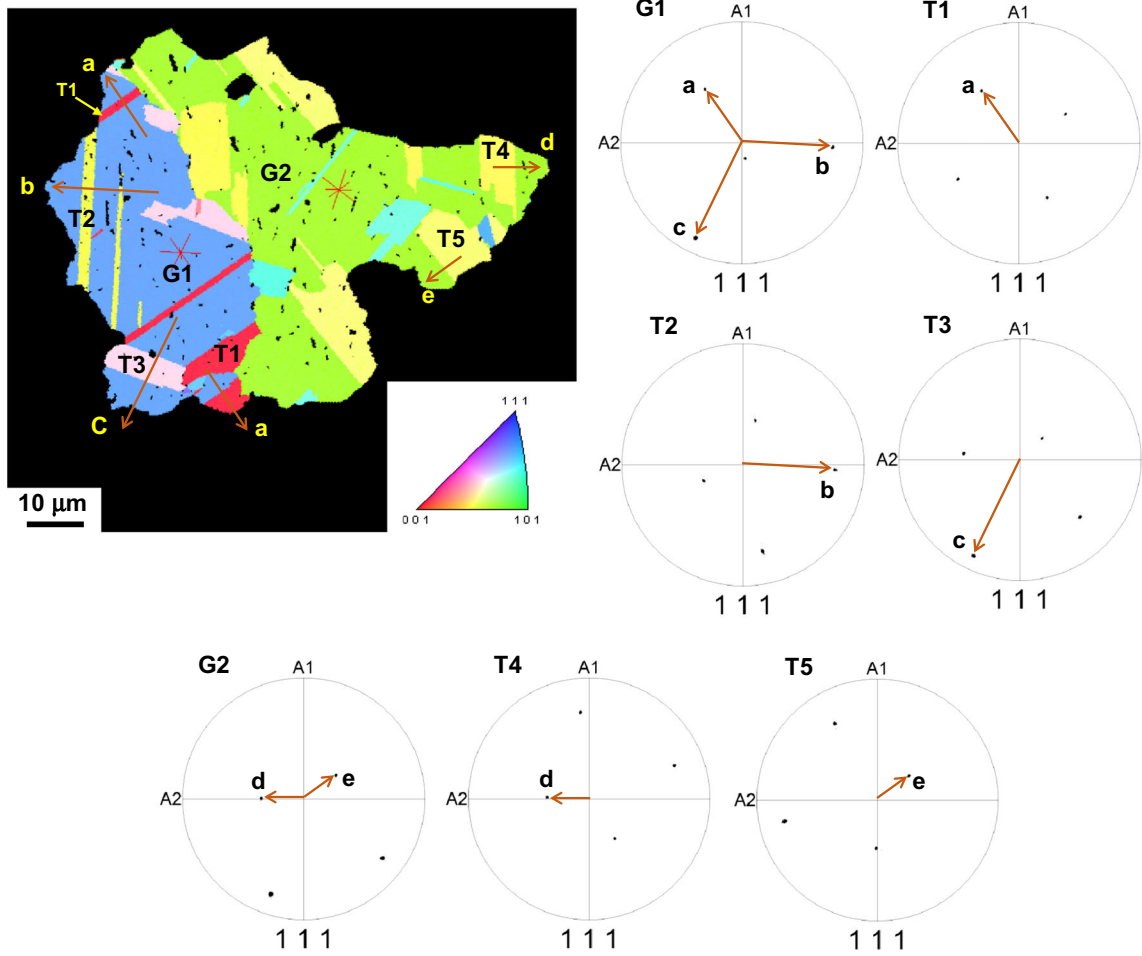


Fig. 9—IPF map of the recrystallized grain of the solution-heat-treated specimen B exposed to a plastic strain of 0.05 after deformation at a displacement rate of 42 mm/s, and $\{111\}$ PFs for the individual parent grains (G1 and G2) and the individual twins (T1 through T5) in the recrystallized grain.

With regard to the present study and the relationship between the formation of the abnormally large grains and twinning, grain boundary migration occurred not only in a direction perpendicular to the $\Sigma 3 \{111\}$ twin boundary but also in a direction parallel to the $\Sigma 3 \{111\}$ twin boundary (Figures 9 through 11). It was proposed that the twinning mechanism was based on the growth accident model of Mahajan *et al.*,^[23] which can express the formation of a twin boundary parallel or perpendicular to the growth front. However, concerning growth in the $\langle 111 \rangle$ direction, there was a local grain boundary movement through higher-order twinning while changing the bulging direction, which caused part of the crystal grain to develop into branches. Thus, this did not appear to contribute to prominent grain coarsening. On the other hand, growth in the $\langle 110 \rangle$ direction parallel to the $\Sigma 3 \{111\}$ twin boundary was

also observed, indicating that the main grain boundary movement by which abnormally large grains developed was growth in this direction along the twin boundary. Figures 13(a) and (b), arrangement schematic diagrams showing octahedrons surrounded by $\{111\}$ planes, demonstrate the arrangement relationship between the parent grain and primary secondary twin, along with the arrangement relationship between the parent grain and two different primary twins, respectively. The common $\langle 110 \rangle$ exists in both. It is supposed that the parent grain, the primary twin, and the secondary twin have different crystallographic orientations but easily grow in the common $\langle 110 \rangle$ direction because the arrangement of atoms is consistent. Moreover, the twin boundary energy is very low and the atom density in this direction is relatively high. The other important role played by twins involves effecting a change in the high-angle

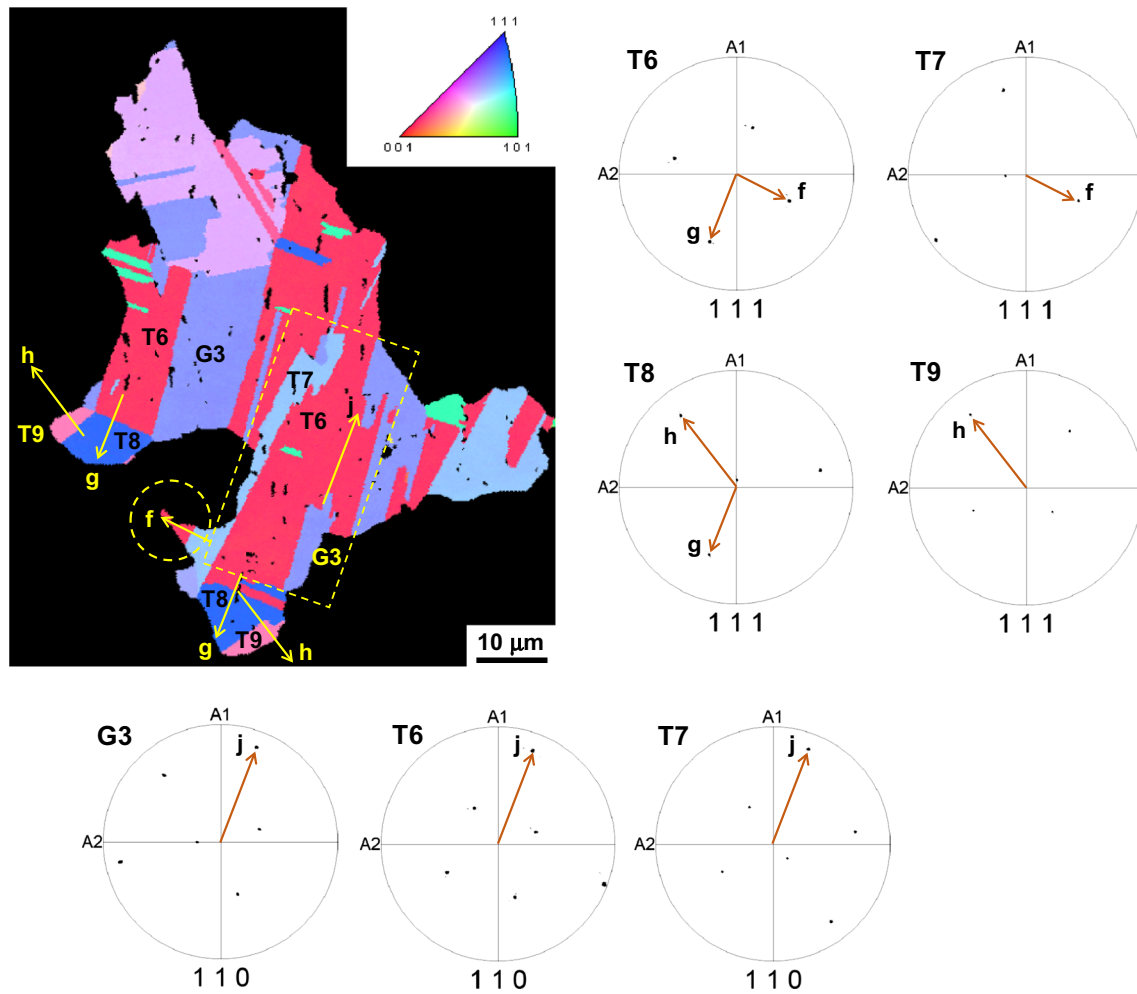


Fig. 10—IPF map of the recrystallized grain for the solution-heat-treated specimen B exposed to a plastic strain of 0.12 after deformation at a displacement rate of 0.42 mm/s, and $\{111\}$ and $\{110\}$ PFs for the parent grain (G3) and the individual twins (T6 through T9) in the recrystallized grain.

boundary to a low-angle boundary, resulting in the coalescence of neighboring grains. This is considered to be a mechanism based on the grain boundary dissociation model proposed by Meyers and Murr.^[25]

V. CONCLUSIONS

The initiation and progress behavior of abnormally large grains in superalloy 718 with an initial grain size of approximately $12\ \mu\text{m}$ in diameter was investigated through hot working and subsequent processes. The results are summarized as follows.

1. A very small number of recrystallized grains coarsened during heat treatment, inducing an abnormally large-grained microstructure. Abnormally large grains were formed through the recrystallization phenomenon.
2. Abnormally large-grained microstructures consisting of larger grains of more complex morphology developed when exposed to a decreased plastic strain. Abnormally large grains grew through multiple twinning.
3. The formation of twins also acted toward partially converting high-angle boundaries to low-angle boundaries.

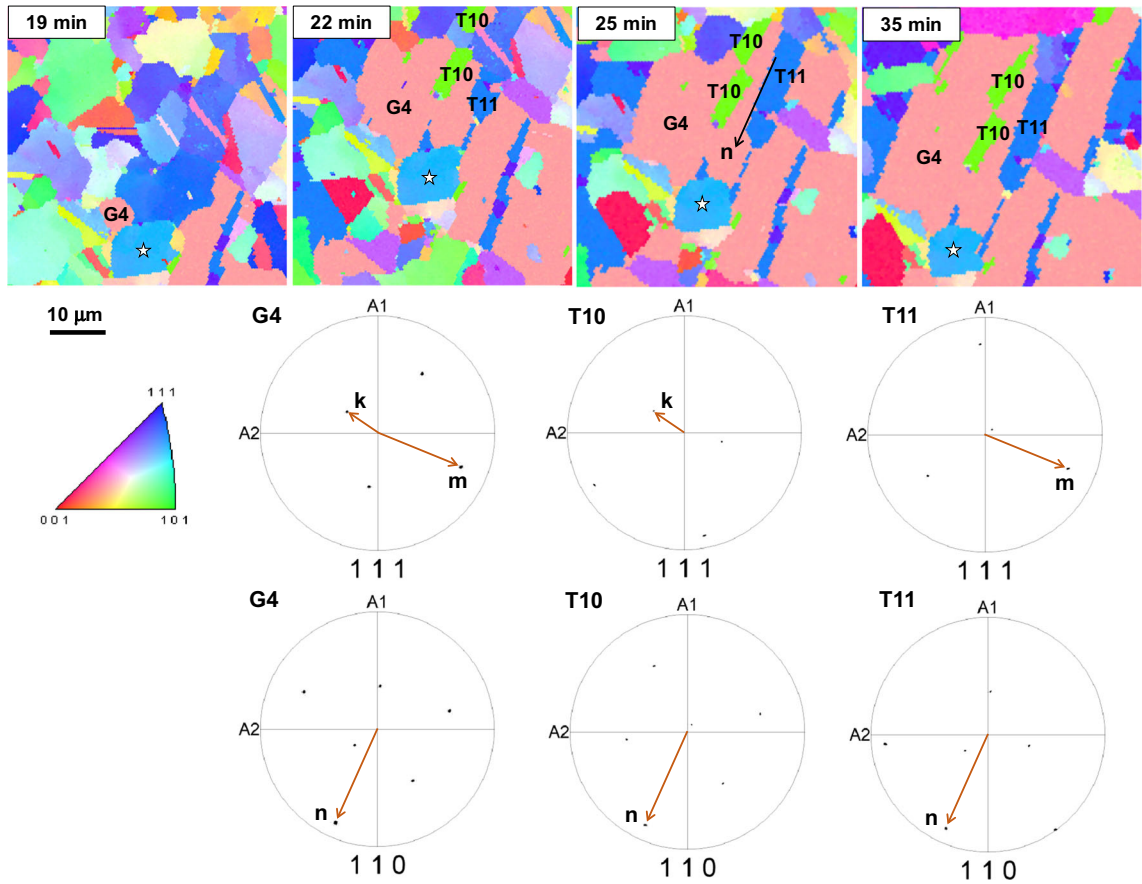


Fig. 11—EBSD results measured during *in-situ* annealing of the specimen B sample exposed to a plastic strain of 0.12 and deformed at 980 °C at a displacement rate of 0.42 mm/s. IPF maps at 19, 22, 25, and 35 min of annealing at 980 °C, respectively. {110} PFs are for the parent grain (G4) and the individual twins (T10 and T11) in the recrystallized grain.

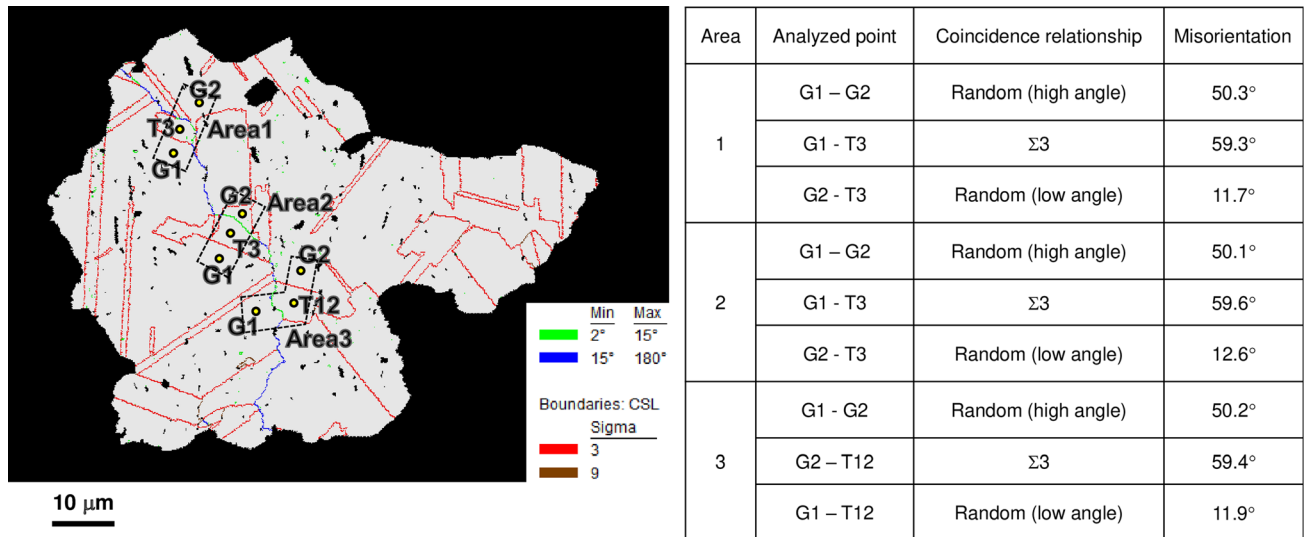


Fig. 12—Grain boundary image of the recrystallized grain, and the relationship between each pair of points near the boundary between the parent grains G1 and G2 for the solution-heat-treated specimen B exposed to a plastic strain of 0.05 after deformation at a displacement rate of 42 mm/s.

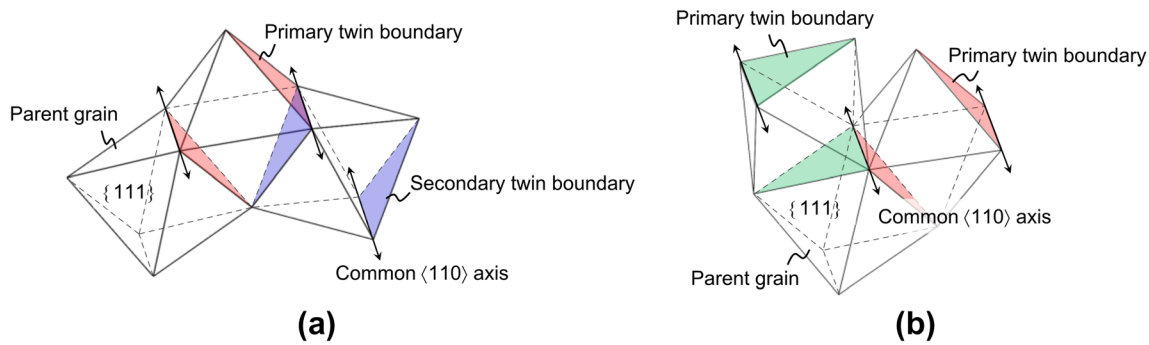


Fig. 13—Illustration of regular octahedron arrangement surrounded by the $\{111\}$. (a) The parent grain, primary twin, and secondary twin. (b) The parent grain and two different primary twins.

ACKNOWLEDGMENTS

This work was supported by the Council for Science, Technology and Innovation (CSTI), Cross-ministerial Strategic Innovation Promotion Program (SIP), and “Structural Materials for Innovation” (Funding agency: JST).

REFERENCES

1. B. Pieraggi and J.F. Uginet: in *Superalloys 718, 625, 706 and Various Derivatives*, E.A. Loria, ed., TMS, Warrendale, PA, 1994, pp. 535–44.
2. J.F. Uginet and B. Pieraggi: in *Superalloys 718, 625, 706 and Various Derivatives*, E.A. Loria, ed., TMS, Warrendale, PA, 1997, pp. 343–52.
3. R. Watson, M. Preuss, J. Quinta de Fonseca, T. Witulski, and G. Terlinde: in *Superalloys 718, 625, 706 and Various Derivatives*, E.A. Loria, ed., TMS, Warrendale, PA, 2014, pp. 873–84.
4. A. Agnoli, M. Bernacki, R. Logé, J.M. Franchet, J. Laigo, and N. Bozzolo: in *Superalloys 2012*, E.S. Huron et al., eds., TMS, Warrendale, PA, 2012, pp. 73–82.
5. A. Agnoli, M. Bernacki, R. Logé, J.M. Franchet, J. Laigo, and N. Bozzolo: *Metall. Mater. Trans. A*, 2015, vol. 46A, pp. 4405–21.
6. R. Schwant, S. Thamboo, L. Yang, and M. Morra: in *Superalloys 718, 625, 706 and Various Derivatives*, E.A. Loria, ed., TMS, Warrendale, PA, 2005, pp. 15–24.
7. C. Aoki, T. Ueno, and T. Ohno: in *Superalloys 2016*, M. Hardy et al., eds., TMS, Warrendale, PA, 2016, pp. 609–17.
8. C. Aoki, T. Ueno, T. Ohno, and K. Oikawa: *J. Mater. Process. Technol.*, 2019, vol. 267, pp. 26–33.
9. B. Flageolet, O. Yousfi, Y. Dahan, P. Villechaise, and J. Cormier: in *Superalloys 718, 625, 706 and Various Derivatives*, E.A. Loria, ed., TMS, Warrendale, PA, 2010, pp. 595–606.
10. E. Huron, S. Srivatsa, and E. Raymond: *Superalloys 2000*, T.M. Pollock et al., TMS, Warrendale, PA, 2000, pp. 49–58.
11. V.M. Miller, A.E. Johnson, C.J. Torbet, and T.M. Pollock: *Metall. Mater. Trans. A*, 2016, vol. 47A, pp. 1566–74.
12. I.M.D. Parr, T.J. Jackson, M.C. Hardy, D.J. Child, C. Argyrakos, K. Severs, V. Saraf, and J.M. Stumpf: in *Superalloys 2016*, M. Hardy et al., eds., TMS, Warrendale, PA, 2016, pp. 447–56.
13. M.A. Charpagne, J.M. Franchet, and N. Bozzolo: *Mater. Des.*, 2018, vol. 144, pp. 353–60.
14. T.A. Bennett, P.N. Kalu, and A.D. Rollett: *Scripta Mater.*, 2007, vol. 57, pp. 41–44.
15. T.A. Bennett, P.N. Kalu, and A.D. Rollett: *Microsc. Microanal.*, 2011, vol. 17, pp. 362–67.
16. T. Watanabe and S. Tsurekawa: *Acta Mater.*, 1999, vol. 47, pp. 4171–85.
17. C.A. Schuh, M. Kumar, and W.E. King: *Acta Mater.*, 2003, vol. 51, pp. 687–700.
18. V. Randle: *Acta Mater.*, 2004, vol. 52, pp. 4067–81.
19. D.B. Bober, J. Lind, R.P. Mulay, T.J. Rupert, and M. Kumar: *Acta Mater.*, 2017, vol. 129, pp. 500–09.
20. C.M. Barr, A.C. Leff, R.W. Demott, R.D. Doherty, and M.L. Taheri: *Acta Mater.*, 2018, vol. 144, pp. 281–91.
21. T.S. Prithiv, P. Bhuyan, S.K. Pradhan, V.S. Sarma, and S. Mandal: *Acta Mater.*, 2018, vol. 146, pp. 187–201.
22. H. Gleiter: *Acta Metall.*, 1969, vol. 17, pp. 1421–28.
23. S. Mahajan, C.S. Pande, M.A. Imam, and B.B. Rath: *Acta Mater.*, 1997, vol. 45, pp. 2633–38.
24. W.G. Burgers: *Physica*, 1949, vol. 15, pp. 92–106.
25. M.A. Meyers and L.E. Murr: *Acta Metall.*, 1978, vol. 26, pp. 951–62.
26. Y. Jin, B. Lin, A.D. Rollett, G.S. Rohrer, M. Bernacki, and N. Bozzolo: *J. Mater. Sci.*, 2015, vol. 50, pp. 5191–5203.
27. D.G. Brandon: *Acta Metall.*, 1969, vol. 14, pp. 1479–84.

Publisher’s Note Springer Nature remains neutral with regard to jurisdictional claims in published maps and institutional affiliations.